PROCEEDINGS OF SPIE

SPIEDigitalLibrary.org/conference-proceedings-of-spie

An optically-transparent transducer with a high-NA and wide-bandwidth for photoacoustic microscopy (PAM)

Fang, Cheng, Zou, Jun

Cheng Fang, Jun Zou, "An optically-transparent transducer with a high-NA and wide-bandwidth for photoacoustic microscopy (PAM)," Proc. SPIE 11642, Photons Plus Ultrasound: Imaging and Sensing 2021, 116421W (5 March 2021); doi: 10.1117/12.2576834



Event: SPIE BiOS, 2021, Online Only

An Optically-Transparent Transducer with a High-NA and Wide-Bandwidth for Photoacoustic Microscopy (PAM)

Cheng Fang and Jun Zou

Dept. of Electrical and Computer Engineering, Texas A&M University, College Station, TX, USA 77843-3128

ABSTRACT

In photoacoustic microscopy (PAM), the ultrasound transducer plays a critical role in detecting the PA signals. However, conventional ultrasound transducers are optically opaque, which could hinder the effective delivery of the excitation laser onto the target. Recently, optically-transparent ultrasound transducers have been investigated to address this issue. Nevertheless, the transparent transducers demonstrated so far have either a small numerical aperture (NA) or narrow bandwidth, which limits their acoustic focal spot sizes and therefore achievable spatial resolutions. In this paper, we report a new focused transparent polyvinylidene fluoride (PVDF) transducer with a high NA of 0.64 and a wide acoustic pulse-echo bandwidth of 120%. Experiment characterization shows that it has an acoustic center frequency and bandwidth of 36 MHz and 44 MHz, respectively. The acoustic focal diameter and zone are 37.8 μ m and 210 μ m, respectively. With the new transparent transducer, dual-modal acoustic-resolution PAM (AR-PAM) and pulse-echo ultrasound microscopy (PE-USM) have been demonstrated with a target consisting of black-ink-filled polyimide tubing buried in chicken breast at different depths. The imaging results show that both the (acoustic) lateral and axial resolutions can be maintained even at a penetration depth of larger than 3 mm.

Keywords: Optically-transparent transducer, high numerical aperture, wide bandwidth, photoacoustic microscopy

1. INTRODUCTION

As a hybrid imaging modality, photoacoustic microscopy (PAM) combines rich optical contrast with deep acoustic penetration beyond the optical diffraction limit [1,2]. To conduct PAM, tightly or loosely focused laser pulses are incident on the surface of a target to excite high-frequency and wide-band PA signals, which are usually detected by a focused ultrasound transducer. To avoid excessive attenuation of the PA signals, the ultrasound transducer needs to be positioned near the target. However, this could cause a difficulty in the light delivery, which can be completely blocked by the ultrasound transducer. To address this issue, an optical and acoustic combiner was developed to separate the optical and acoustic paths [3,4], which however makes the PAM system more complex and bulkier. As an alternative approach, hollow or ring transducers have been used in PAM to allow the laser to directly pass through [5,6]. Nevertheless, with the center part removed, the acoustic sensitivity and focusing capability of the transducers are compromised. Recently, planar or unfocused transducers made of optically-transparent substrates [7-14] have been investigated. However, without a well-defined acoustic focal point, they do not provide an optimal detection condition for the PA signals. More recently, an optically-transparent focused transducer has been developed for combined photoacoustic and ultrasound microscopy [15]. However, limited by the relatively narrow bandwidth due to the rigid piezoelectric material and non-ideal backing, it could not provide an optimal acoustic axial resolution.

Previously, we demonstrated an optically-transparent focused transducer consisting of a PVDF (polyvinylidene fluoride) layer with central indium-tin oxide (ITO) and surrounding metal electrodes [16]. The transducer film was molded onto a concave glass lens, which provides a numerical aperture (NA) of 0.23. However, its acoustic sensitivity and spatial resolution are limited by the coupling factor of PVDF and more importantly its relatively low NA. To solve this problem, we report the development of a new optically-transparent focused PVDF transducer with a high NA of 0.64. Our testing results show that with a higher NA, the acoustic performance of the transducer has been significantly improved. To demonstrate its application in both PAM and pulse-echo ultrasound microscopy (PE-USM), a compact dual-modal imaging setup has been built and imaging experiments have been conducted on ink-filled tubing buried inside chicken breast tissue. The imaging results show that the new high-NA transparent PVDF transducer can provide good acoustic sensitivity and spatial resolution at a penetration depth of ≥ 3 mm.

Photons Plus Ultrasound: Imaging and Sensing 2021, edited by Alexander A. Oraevsky Lihong V. Wang, Proc. of SPIE Vol. 11642, 116421W ⋅ © 2021 SPIE CCC code: 1605-7422/21/\$21 ⋅ doi: 10.1117/12.2576834

2. TRANSDUCER DESIGN AND CONSTRUCTION

To construct the high-NA PVDF transparent transducer, a piece of flat 9-μm-thick PVDF film was molded by a pair of matched convex and concave glass lenses. The ITO electrode was deposited onto the central region of the convex side of the molded PVDF film, and then the chrome / copper electrode was deposited outside the central transparent area. The convex side with electrode of the PVDF film was bonded onto the spherical surface of the concave lens with an UV epoxy. After this, the same electrode deposition process was repeated on the concave side of the PVDF film. Fig. 1 shows a fabricated prototype of the high-NA transparent PVDF transducer. The concave glass lens has a diameter of 12.0 mm and a spherical radius (acoustic focal length) of 9.4 mm, which corresponds to an NA of 0.64. The central transparent region (with a diameter of 3.0 mm) of the transducer is covered with ITO electrodes, while the remaining portion has chrome / copper electrodes to reduce the electrical resistance. The optical transmittance of the central transparent region was around 60% at 532 nm, which is similar with the previous low-NA transducer [16]. To generate a well-defined focal point even with higher NA, the molding and bonding processes of the transducer were optimized to avoid any wrinkles or bubbles formed on the spherical surface of the transducer.

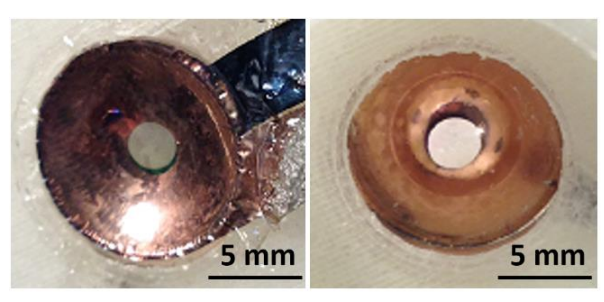


Figure 1. The photographs of the front (on left) and back (on right) sides of a fabricated prototype transducer.

3. TRANSDUCER TESTING AND CHARACTERIZATION

Pulse-echo ultrasound testing was conducted to characterize the acoustic performance of the high-NA transparent PVDF transducer. The transducer was driven by a pulser-receiver (Olympus NDT, USA) with a 200 Hz repetition rate. The transmitted ultrasound pulses were incident onto the sharp edge of a razor blade immersed in water. After the propagation along the reversal path, the reflected or backscattered ultrasound signals were received by the transducer itself and amplified by the preamplifier embedded in the pulser-receiver. The amplified pulse-echo signal and its frequency spectrum (Fig. 2 (a)) were used to determine the center frequency (f_c) and bandwidth (BW), indicating an f_c and a 3-dB pulse-echo BW of 36 MHz and 44 MHz, respectively, which results in a calculated acoustic axial resolution of 8.75 μ m. The f_c and BW are slightly higher than those obtained from the previous low-NA transducer [16], possibly due to better construction and the use of a finer target.

To determine the acoustic focal spot and focal zone (depth of focus) of the high-NA transparent PVDF transducer, the pulse-echo ultrasound testing was repeated by scanning the razor blade along both X and Z axes around the (estimated) focal point. The scanning range along X axis was $80 \mu m$ with a step size of $2 \mu m$. The scanning range along Z axis is $300 \mu m$ with a step size of $10 \mu m$. At each height, the amplitude of the echo signal from the razor blade was recorded and normalized. The FWHM (full width at half maximum) value of the Gaussian-fitted amplitude profile was used to determine the corresponding acoustic beam diameter (Fig. 2 (b)). After repeating the horizontal scan at different heights, the acoustic focal spot was determined by the minimal FWHM, and the acoustic depth of focus was estimated by the height range where the on-axis peak amplitude dropped to half of its maximal value [17]. As listed in Table 1, the acoustic focal spot size and focal zone of the transducer were determined to be $37.8 \mu m$ and $210 \mu m$, respectively.

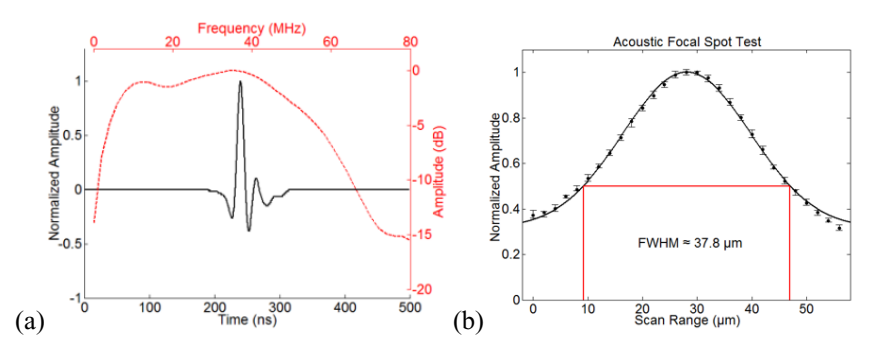


Figure 2. (a) A representative echo signal (in black) and its frequency spectrum (in red). (b) The minimal FWHM of the Gaussian-fitted profile of the echo signal amplitude along X axis.

Table 1. Measured acoustic focal spot diameter and peak amplitude at different heights

| Height H (mm) | FWHM (µm) | Normalized Peak Amplitude |
|---------------|-----------|---------------------------|
| 7.49 | 67.6 | 0.50 |
| 7.58 | 37.8 | 1.00 |
| 7.70 | 67.0 | 0.49 |

4. IMAGING EXPERIMENTS AND RESULTS

To demonstrate its imaging capability, the high-NA transparent PVDF transducer was used to conduct both acousticresolution PAM (AR-PAM) and PE-USM with a dual-modal imaging setup (Fig. 3). For AR-PAM, a 532-nm pulsed laser (Elforlight, UK) triggered by a function generator with 1-kHz repetition rate was used as the light source. The output laser beam was expanded, passed through a beam splitter, reflected by a stationary mirror, and focused by a lens with 10-cm focal length. The loosely focused laser beam propagated through the transducer onto the target. A CCD camera was used to monitor the excitation region through the reverse path of the optical illumination. Laser pulse energy after the transparent transducer was measured to be 35 µJ, and the laser spot diameter onto the top surface of the target was around 1 mm, which corresponds to a laser intensity of 4.5 mJ/cm², far below the ANSI limit of 20 mJ/cm². Because the laser illumination spot is much larger than the acoustic focal spot of the transducer, the lateral resolution of the PAM is determined acoustically by the focal spot size of the transducer. For PE-USM, a pulser-receiver (Olympus NDT, USA) was synchronously triggered by the same function generator to drive the transducer for sending ultrasound pulses to the target. Therefore, one trigger from the function generator would initiate simultaneous PA and ultrasound data acquisition, which helps to improve the imaging speed. Both the target and the front spherical surface of the transducer were immersed in a water tank, which was placed onto a computer-controlled X/Y motor stage and a manually-adjusted Z stage. The PA and ultrasound signals received by the transducer were amplified by the preamplifier embedded in the pulser-receiver and then recorded by a data-acquisition card (Alarzar Tech, Canada). It should be noted that this single triggering scheme will not cause the mixing of PA and ultrasound signals. Upon excitation, the ultrasound signal goes through a round trip (from the target to the transducer) and reaches the transducer, while the PA signal arrives after a single trip. The time delay of the ultrasound signal will be twice that of the PA signal (~6 µs) determined by the acoustic focal length (~9 mm) of the transducer and the acoustic velocity (~1500 m/s) in water. Because the difference in their time delay (~6 μs) is much longer than their duration (0.1~0.2 µs), both the PA and ultrasound signals are completely separated in time domain and therefore can be received without any mixing.

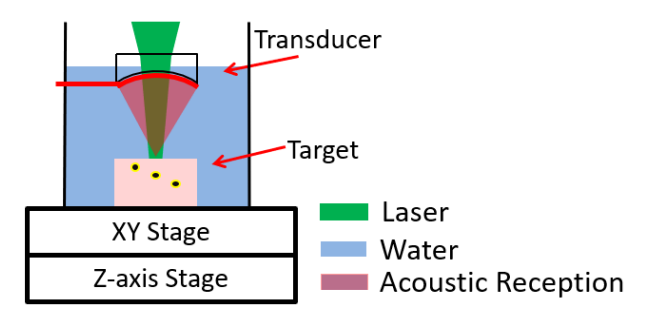


Figure 3. Schematic of the dual-modal imaging setup with the high-NA transparent PVDF transducer.

For the imaging experiment, three polyimide tubing were used as the target, which were filled with black ink and buried inside a piece of chicken breast. The depths of the three tubing are 1, 2 and 3 mm, respectively. The lateral spacing between two adjacent tubing is 3 mm (Fig. 4). A total area of 8×0.5 mm² (marked by the white dashed rectangle in Fig. 4 (a)) was scanned with a step size of 10 μ m and 5 μ m along X and Y axis, respectively. At each location, the data acquisition was repeated 10 times and the acquired PA and ultrasound signals were averaged to improve the signal-to-noise ratio (SNR). To reduce the imaging time, the PA and ultrasound data were acquired at three different depths (1, 2 and 3 mm), where the top, middle, and bottom tubing was aligned with the acoustic focal point of the transducer, respectively. Fig. 5 shows the representative PA & pulse-echo ultrasound signals received from the polyimide tubing at different depths. The amplitude of the PA signals drops quickly with depth of the tubing, which is caused by the strong optical absorption and scattering by the chicken breast at a relatively short wavelength of 532 nm. In contrast, the amplitude of the ultrasound signals remains almost the same, which is due to the weak acoustic attenuation and scattering in the chicken breast at a depth of a few mm. The small signals after the main pulse are caused by the acoustic reflection inside the glass lens.

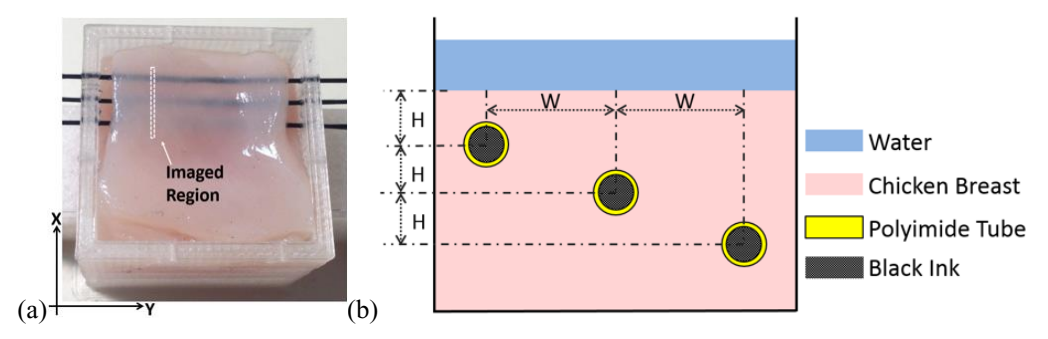
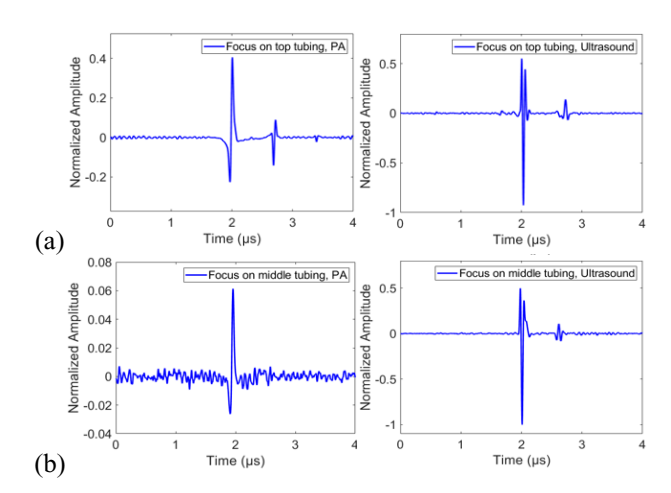


Figure 4. (a) Photo of the three black-ink-filled polyimide tubing buried in chicken breast. The imaged region is marked by the white dashed rectangle. (b) Diagram of the tubing in chicken breast. W = 3.0 mm, W = 1.0 mm.



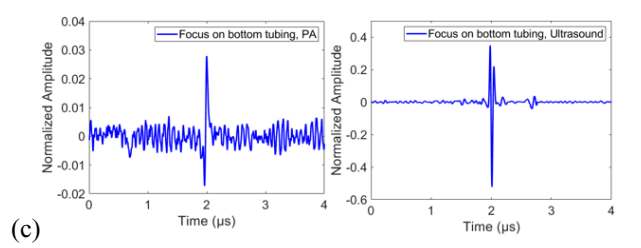


Figure 5. Representative PA (left column) & pulse-echo ultrasound (right column) signals with transducer focusing at the (a) top, (b) middle, and (c) bottom black-ink-filled polyimide tubing in chicken breast. The time duration is cropped to show the details of the two signals.

Fig. 6 shows the B-scan PA and ultrasound maximum amplitude projection (MAP) images when the tubing at the top, middle, and bottom was in (acoustic) focus, respectively. The C-scan PA and ultrasound MAP images are shown in Fig. 7. The PA and ultrasound images were reconstructed based on the signal amplitude at each scan point, which is represented by the grayscale of the corresponding pixel. As shown in the PA images, the tubing at the top generates the strongest PA signals even if it is out of focus. This is because the strong optical absorption and more importantly, the optical scattering in chicken breast tissue cause the excitation laser intensity to drop quickly at larger penetration depths. The contrast ratio (CNR) of the PA images drops from 36 dB (when the tubing at the top is in focus) to 24.7 dB (when the tubing at the bottom is in focus). Nevertheless, the tubing which is in focus is resolved clearly while the other two (out of focus) appear blurry. Therefore, targets at different depths could still be differentiated, due to the good spatial resolution enabled by the high-NA transparent PVDF transducer. In contrast, as shown in the ultrasound images, the tubing in focus is resolved clearly while the other two are barely seen. The CNR remains around 40 dB at different imaging depths. This can be explained by the fact that the chicken breast tissue has low acoustic attenuation and scattering. As a result, both ultrasound excitation and detection are all directed to the focal point.

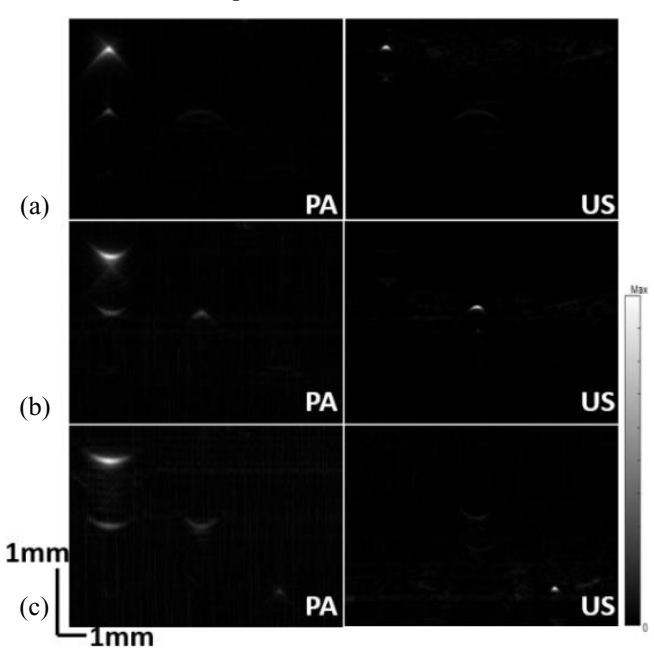


Figure 6. The reconstructed B-scan PA (left column) and pulse-echo ultrasound (right column) MAP images with acoustic focusing on the (a) top, (b) middle, and (c) bottom polyimide tubing buried in chicken breast.

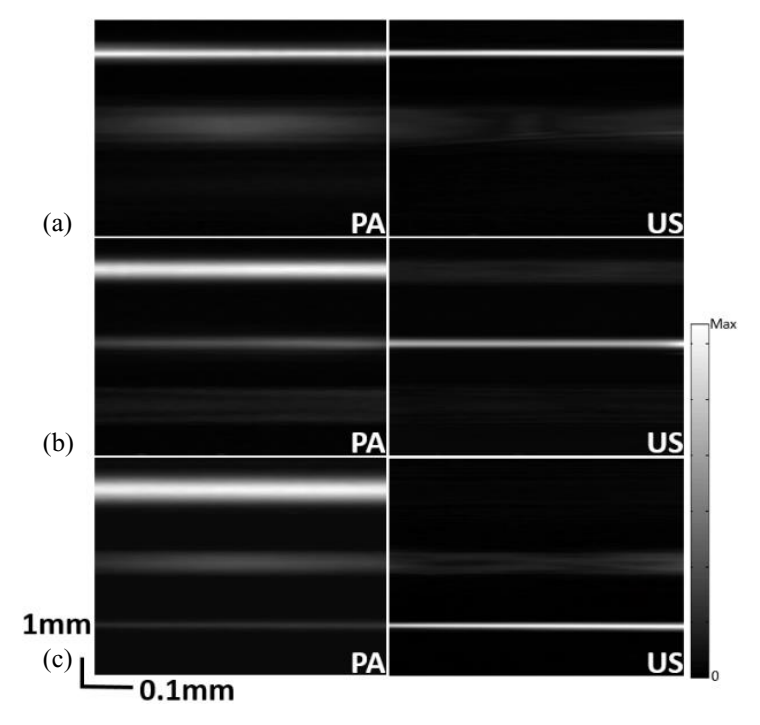


Figure 7. The reconstructed C-scan PA (left column) and pulse-echo ultrasound (right column) MAP images with acoustic focusing on the (a) top, (b) middle, and (c) bottom polyimide tubing buried in chicken breast.

5. SUMMARY AND CONCLUSION

In summary, a new optically-transparent focused PVDF ultrasound transducer has been designed, fabricated and characterized. Its application in dual-modal photoacoustic and pulse-echo ultrasound microscopy has been demonstrated. With a high NA, a wide acoustic bandwidth and also good optical transparency, the transducer can provide a small acoustic focal spot and therefore a high acoustic resolution without light blockage. Such capabilities can be useful for the development of compact dual-modal acoustic microscopy systems for handheld, wearable and even endoscopic imaging applications.

ACKNOWLEDGMENTS

This work is supported in part by awards (NRI-1748161and NRI-1925037) from the National Science Foundation. Any opinions, findings, conclusions, or recommendations presented are those of the authors and do not necessarily reflect the views of the National Science Foundation.

REFERENCES

- [1] Wang, L. V., [Photoacoustic imaging and spectroscopy], CRC press (2017).
- [2] Wang, L. V. and Yao, J., "A practical guide to photoacoustic tomography in the life sciences," Nature methods 13(8), 627 (2016).
- [3] Maslov, K., Zhang, H. F., Hu, S. and Wang, L. V., "Optical-resolution photoacoustic microscopy for in vivo imaging of single capillaries," Optics letters 33(9), 929-931 (2008).
- [4] Hu, S., Yan, P., Maslov, K., Lee, J. M. and Wang, L. V., "Intravital imaging of amyloid plaques in a transgenic mouse model using optical-resolution photoacoustic microscopy," Optics letters 34(24), 3899-3901 (2009).

- [5] Wang, T., Sun, N., Cao, R., Ning, B., Chen, R., Zhou, Q. and Hu, S., "Multiparametric photoacoustic microscopy of the mouse brain with 300-kHz A-line rate," Neurophotonics 3(4), 045006 (2016).
- [6] Lan, B., Liu, W., Wang, Y.C., Shi, J., Li, Y., Xu, S., Sheng, H., Zhou, Q., Zou, J., Hoffmann, U., Yang, W. and Yao, J., "High-speed widefield photoacoustic microscopy of small-animal hemodynamics," Biomedical optics express 9(10), 4689-4701 (2018).
- [7] Brodie, G. W., Qiu, Y., Cochran, S., Spalding, G. C. and Macdonald, M. P., "Optically transparent piezoelectric transducer for ultrasonic particle manipulation," IEEE transactions on ultrasonics, ferroelectrics, and frequency control 61(3), 389-391 (2014).
- [8] Hata, T., Sato, Y., Nagai, Y. and Hada, T., "Photoacoustic Measurement of CdS by Transparent Transducer Method," Japanese Journal of Applied Physics 23(S1), 75 (1984).
- [9] Niederhauser, J. J., Jaeger, M., Hejazi, M., Keppner H. and Frenz, M., "Transparent ITO coated PVDF transducer for optoacoustic depth profiling," Optics communications 253(4-6), 401-406 (2005).
- [10] Buchberger, G., Barb, R. A., Schoeftner, J., Bauer, S., Hilber, W., Mayrhofer, B. and Jakoby, B., "Transparent, flexible, thin sensor surfaces for passive light-point localization based on two functional polymers," Sensors and Actuators A: Physical 239, 70-78 (2016).
- [11] Beard, P. C., Perennes, F. and Mills, T. N., "Transduction mechanisms of the Fabry-Perot polymer film sensing concept for wideband ultrasound detection," ieee transactions on ultrasonics, ferroelectrics, and frequency control 46(6), 1575-1582 (1999).
- [12] Zhang, E., Laufer, J. and Beard, P., "Backward-mode multiwavelength photoacoustic scanner using a planar Fabry-Perot polymer film ultrasound sensor for high-resolution three-dimensional imaging of biological tissues," Applied optics 47(4), 561-577 (2008).
- [13] Li, Z., Ilkhechi, A. K. and Zemp, R., "Transparent capacitive micromachined ultrasonic transducers (CMUTs) for photoacoustic applications," Optics express 27(9), 13204-13218 (2019).
- [14] Li, H., Dong, B., Zhang, Z., Zhang, H. F. and Sun, C., "A transparent broadband ultrasonic detector based on an optical micro-ring resonator for photoacoustic microscopy," Scientific reports 4, 4496 (2014).
- [15] Park, S., Kang, S., and Chang, J. H., "Optically Transparent Focused Transducers for Combined Photoacoustic and Ultrasound Microscopy," Journal of Medical and Biological Engineering, 1-12 (2020).
- [16] Fang, C., Hu, H. and Zou, J., "A Focused Optically Transparent PVDF Transducer for Photoacoustic Microscopy," IEEE Sensors Journal 20(5), 2313-2319 (2019).
- [17] Olympus, "Ultrasonic Transducers Technical Notes," 2006, https://mbi-ctac.sites.medinfo.ufl.edu/files/2017/02/ultrasound-basics.pdf (2006).